An Almahata Sitta EL3 fragment: Implications for the Unique Thermal History of Enstatite Chondrites

Makoto Kimura (kimura.makoto@nipr.ac.jp)
National Institute of Polar Research https://orcid.org/0000-0003-3352-4989
Michael K. Weisberg
Kingsborough Community College
Asako Takaki
Ibaraki Daigaku
Naoya Imae
National Institute of Polar Research Division for Research and Education: Kokuritsu Kyokuchi Kenkyujo Kenkyu Kyoikukei
Akira Yamaguchi
National Institute of Polar Research Division for Research and Education: Kokuritsu Kyokuchi Kenkyujo Kenkyu Kyoikukei

Research article

Keywords: enstatite chondrite, breccia, thermal history, opaque minerals

Posted Date: March 13th, 2021

DOI: https://doi.org/10.21203/rs.3.rs-300648/v1

Abstract

Almahata Sitta is a polymict breccia, consisting of many kinds of clasts. Here we present our mineralogical and petrological results on an EL3 fragment, MS-177 from Almahata Sitta. This fragment shows a typical type 3 chondritic texture, consisting of well-defined chondrules often with olivine, isolated silicate minerals, and opaque nodules. Although these components are typical of EL3 chondrites, the mineral abundances and compositions are different from the other EL3s. Diopside is highly abundant. On the other hand, perryite and daubreelite were not found. The major pyroxene is orthoenstatite, and the silica phase is quartz. Fe-Ni metal has relatively high P contents. Troilite is enriched in Cr and Mn. Keilite and buseckite are present in MS-177. From the mineralogy and texture, MS-177 experienced a high-temperature event under subsolidus conditions. Shock-induced heating for a short duration might explain this high-temperature event. This is supported by shock-induced darkened feature of MS-177. We suggest that other E3 chondrites also experienced heating events under such subsolidus conditions on their parent bodies. On the other hand, the high abundance of diopside cannot be explained by a secondary thermal event and may have been a primary feature of MS-177, formed before accretion to the parent body.

1. Introduction

Almahata Sitta fell in northern Sudan on October 7, 2008 and is an unusual polymict breccia consisting of various kinds of fragments, such as ureilitic and chondritic (e.g., Horstmann and Bischoff 2014). The chondritic fragments include enstatite (E), ordinary, carbonaceous, and R-like chondrites. E chondritic fragments include EH3-6, EL3-6, and impact melt rocks. Here we present our mineralogical and petrological results on an E chondrite fragment, MS-177. El Goresy et al. (2012) classified it as an EL3. Especially, they studied opaque nodules in this fragment and another MS-17 and discussed the condensation processes, especially of oldhamite and sinoite in the early solar nebula.

We also investigated MS-177 and noticed that this fragment experienced a unique thermal history. This is important for elucidating the complicated thermal history of E chondrites. Here we will discuss the thermal history of the MS-177, especially on the EL3 parent body. We compare the results of the MS-177 with another EL3 chondrite, Asuka (A) 881314 and a heavily shocked EH3 chondrite, Asuka (A) 10164 (Kimura et al. 2017). A 10164 has a shock vein containing coesite, indicating that it experienced 3–10 GPa and 1000°C. The host was also heated at < 1000°C during the shock event.

It is difficult to evaluate the thermal histories of E chondrites, especially their subsolidus conditions by the silicate minerals. We do not have appropriate silicate geothermometers, except silica polymorphs (Kimura et al. 2005). Instead, some of the opaque minerals typical of E chondrites give quantitative constraints on the physical condition for their thermal histories (e.g., Zhang and Sears 1996; Kimura et al. 2017). In addition, Weyrauch et al. (2018) recently proposed that E chondrites (EH and EL) are divided into a and b subgroups, from the compositions of sulfide minerals which do not depend on petrologic type (i.e., thermal alteration). Such classification is significant in providing hints for the thermal histories of E chondrites. We noticed that the MS-177 fragment experienced high-temperature events under subsolidus conditions. Therefore, we mainly studied opaque minerals in it and expect that these geothermometers can help constrain the thermal history not only of this fragment but also other E chondrites.

2. Sample And Experimental Methods

We investigated a polished thin section of the MS-177 fragment. In comparison, we studied a typical EL 3 chondrite, A-881314, 51 – 1.

Back-scattered electron (BSE) images were obtained using the JEOL JSM-7100F field emission scanning electron microscope (FESEM) at the National Institute of Polar Research (NIPR). Mineral analyses were conducted using the JEOL JXA8200 electron-probe microanalyzer at NIPR with a focused beam. The beam currents were 4 nA for glass, plagioclase, and silica, and 30n A for pyroxene, olivine, and opaque minerals at 15 KeV. The analytical and correction methods were the same as that by Kimura et al. (2017). The X-ray overlaps of K_a on K_b lines of some elements, Fe-Co and Ni-Cu, were corrected with a deconvolution program. We identified some phases using a laser micro Raman spectrometer (JASCO NRS 1000) at the NIPR after the method of Kimura et al. (2017). The elemental X-ray maps of the section were obtained using the FESEM. We determined the modal compositions from elemental maps of the whole areas of the thin section. ImageJ software was used to calculate the modal composition of mineral based on the X-ray intensities of each pixel. Imae et al. (2019) have applied an X-ray diffraction (XRD) method to characterize minerals in meteorite thin sections by using SmartLab, RIGAKU at the NIPR. We used the same method for the identification of pyroxene in the sample studied here.

3. Results

3.1 Petrography

Figures 1a to 1d show the section of MS-177 studied here. MS-177 contains abundant chondrules among isolated silicate minerals, and opaque nodules and isolated minerals. The fine-grained matrix is a minor component and not easily discernible like the other E chondrites (e.g., Weisberg and Kimura 2012). This texture is indicative of type 3 E chondrite which is supported by the occurrence of olivine in chondrules (Weisberg and Kimura 2012; Weyrauch et al. 2018). The opaque minerals in the MS-177 are typical of E chondrites, such as Si-bearing Fe-Ni metal and (Mg,Mn,Fe)S phase (Weisberg and Kimura 2012).

Chondrules abundantly show well-defined outlines and are 0.69 mm in average diameter typical of EL3 chondrites (0.6 mm) (e.g., Jones 2012). Most chondrules are porphyritic (pyroxene-dominated) and a few radial pyroxene types are noticed. Porphyritic chondrules mainly consist of low-Ca pyroxene phenocryst and devitrified mesostasis often with feldspar and a silica phase. Olivine is often noticed poikilitically enclosed within pyroxene phenocryst. One of the characteristic features of the MS-177 is a high abundance of high-Ca pyroxene in chondrules (Figs. 1c and 2a). It is generally not a common mineral in E chondrites. In chondrules of the MS-177, high-Ca pyroxene occurs as coarse-grained phenocrysts, a rim on low-Ca pyroxene phenocryst, and as fine-grained laths associated with feldspar in chondrule mesostases. Fe-Ni metal and troilite with small amounts of (Mg,Mn,Fe)S phase, oldhamite, and (Fe,Zn)S phase are present in some chondrules. Isolated silicate minerals include low-Ca pyroxene, high-Ca pyroxene, feldspar, and a silica mineral.

Opaque minerals in nodules and as isolated minerals are mainly Fe-Ni metal with troilite and rare schreibersite (Fig. 1d). Fe-Ni metal in opaque nodules includes abundant euhedral laths of pyroxene (both low and high-Ca pyroxenes) with feldspar and the oxynitride sinoite (Si_2N_2O; Fig. 2b). Oldhamite and (Mg,Mn,Fe)S phase are rarely encountered in the opaque nodules.

MS-177 shows heavily shock-induced features (S4 after Rubin et al. 1997), such as distinct mosaicism and wavy extinction of pyroxene. However, we found no melt vein in MS-177, which are observed in the A 10164 EH3 chondrite (Kimura et al. 2017). Euhedral laths of enstatite typical of melt rocks (Rubin and Scott 1997; Lin and Kimura 1998; Kimura and Lin 1999) are not encountered in the MS-177 except in opaque nodules. Figure 2c shows the texture of metal and troilite as isolated minerals. They do not show any eutectic intergrowth texture, which is commonly present in a shock melt vein in A 10164 (Kimura et al. 2017). However, it also shows darkening under plane polarized transmitted light in the optical microscope (Fig. 1a). Many silicate phases contain abundant fine-grained opaque minerals resulting in the darkened appearance.

3.2 Modal compositions

Table 1 shows the modal composition of the constituent mineral in the MS-177 and the average EL3 chondrite (Weisberg and Kimura 2012). The most abundant phase is low-Ca pyroxene, as is typical of EL chondrites. In comparison to average EL3 (Weisberg and Kimura 2012), high-Ca pyroxene is highly abundant in the MS-177, whereas olivine is not so abundant. Troilite is slightly more abundant than the average, but within the range of other EL3s. Schreibersite and (Mg,Mn,Fe)S phase are slightly less abundant, and perryite and daubreelite were not found although they are typical minerals in EL chondrites.

3.3 Silicate mineral chemistry

Table 2 shows selected analyses of silicate minerals. Low-Ca pyroxene contains $Fs_{<1.3}$ and $Wo_{<1.4}$ components, whereas high-Ca pyroxene is $Fs_{<1.4}$ and Wo_{43-48}. Hereafter we call them enstatite and diopside, respectively. Enstatite contains < 0.8 wt.% Al_2O_3, and TiO_2, Cr_2O_3, and MnO below detection limits (Table 3). Diopside contains < 0.2 wt.% TiO_2, 0.2–1.1 Al_2O_3, < 0.13 Cr_2O_3, and < 0.12 MnO. In comparison, enstatite in the A-881314 EL3 contains $Fs_{<1.7}$ and $Wo_{<0.8}$, which is consistent with that in the MS-177 fragment. On the other hand, diopside was not found in A-881314.

Olivines both in the MS-177 and A-881314 are $Fa_{<1}$. They contain < 0.15 wt.% MnO, whereas the other minor elements are below detection limits.

Feldspars, both in the MS-177 and A-881314, are albitic, Ab_{61-74} and Ab_{63-91}, respectively. Devitrified glasses in chondrules of the MS-177 contain 12.4–29.2 wt.% Al_2O_3, 0.2–15.2 MgO, 0.8–13 CaO, 2.9–9.5 Na_2O, and 0.2–1.3 K_2O, indicative that they are mainly comprised of feldspar and diopside components. Some devitrified glass contains < 2.4 wt.% Cl. El Goresy et al. (1988) also reported Cl from chondrules in Qingzhen EH3. Chlorine-bearing phases were not identified in the chondrules from MS-177, such as djerfisherite, lawrencite, and hibbingite. Therefore, chlorine is contained in the glassy mesostasis of the MS-177 chondrules.

Silica mineral is nearly pure SiO_2.

3.4 Opaque mineral chemistry

Table 3 shows the selected analyses of opaque minerals. Fe-Ni metal in MS-177 contains 0.3–0.6 wt.% Si, which are within the range of A-881214 and other EL chondrites (Weisberg and Kimura 2012; Fig. 3a). On the other hand, it contains 0.3–0.6 wt.% P and 6.4–7.9 Ni, higher than those in A-881314 (Fig. 3b). This is one of the characteristic features of the MS-177.

Schreibersite contains < 0.2 wt.% Si and 7.0-7.8 wt.% Ni. Although the Si contents are the same as those in A-881314, the Ni contents are much higher than those in A-881314 (Fig. 4).

Troilite contains 2.1–2.6 wt.% Cr, 0.9–1.6 Mn, and 0.3–0.4 Ti. The contents of Mn and Cr are higher than those in A-881314 (Fig. 5a), whereas Ti contents are lower (Fig. 5b).

(Mg,Mn,Fe)S grain is rarely noticed in the MS-177 (Table 3). This is identified as keilite from the composition (Fig. 6). This is in contrast to the occurrence of alabandite in A-881314. Although this keilite contains 7.1 wt.% Cr, daubreelite and another Cr-bearing phase are not noticed. Oldhamite is not a common phase and contains 0.5–0.8 wt.% Mg, 1.1–1.3 Mn, and 0.7-1.0 Fe.

An (Fe,Zn)S grain was found among enstatite in a chondrule (Fig. 2d). It contains 29.1 wt.% Fe and 26.1 Zn. From the chemical composition, the chemical formula of this phase is $(Fe_{0.49}Zn_{0.38}Mn_{0.09}Mg_{0.04})_{1.00}S_1$.

3.5 Raman spectroscopy

By using laser Raman microscopy, we identified the feldspar phase as albite from the typical peaks of 506 and 206 cm^{-1} (Fig. 7a), not kumdykolite, a high-temperature polymorph of albite, in all occurrences. The silica phase is quartz from the peak of 465 cm^{-1} (Fig. 7b). This is different from that in other EL3s which commonly contain tridymite or cristobalite (Kimura et al. 2005).

Figure 7c shows the Raman spectrum of the (Fe,Zn)S phase. The distinct peak of 300 cm^{-1} indicates that this is buseckite, and not rudashevskyite, a low-temperature polymorph of buseckite. This phase was first reported in an enstatite-rich achondrite, Zakłodzie, by Ma et al. (2012). In our knowledge, our finding is the second report of this mineral.

Fe-Ni metal contains sinoite grains which are identified by the peaks of 984, 734, 495, and 456 cm^{-1}, which are consistent with the peaks of sinoite in the Y-793225 E chondrite (Kimura et al. 2005).

3.6 XRD

We identified low-Ca pyroxene by the XRD data. The diffraction peaks of 321, 511, and 610 indices indicate that the pyroxenes are orthoenstatite, not clinoenstatite, in the MS-177 (Fig. 8). Diopside (Dio) is also abundantly identified from the XRD data.

4. Discussion

4.1 Classification

The MS-177 was classified as an EL3 (El Goresy et al. 2012). Our observations support this classification. The average diameter of chondrule and Si contents in Fe-Ni metal and schreibersite are typical of EL chondrites. Although the MS-177 experienced shock metamorphism, the MS-177 still preserves abundant well-defined chondrules with devitrified glassy mesostasis. These features are indicative of type 3. Chondrules also contain olivine. This is the key evidence for type 3 E chondrites (e.g., Weisberg and Kimura 2012; Weyrauch et al. 2018).

Weyrauch et al. (2018) proposed that both EH and EL chondrites are divided into a and b subgroups based on their sulfide compositions, in spite of their petrologic type, since the compositions of sulfides do not depend on petrologic type. From their criteria, the MS-177 is classified as an ELb3, from the compositions of troilite enriched in Cr and Mn.

On the other hand, this fragment has unique features different from the other type 3 E chondrites, such as unusual modal abundances of its constituent minerals and the occurrences of orthoenstatite and quartz. Especially, the high abundance of diopside is a unique feature in E chondrites. A diopside-rich chondrules was reported in Mac Alpine Hills 88136 EL3 chondrites but this only one unusual chondrule (Weisberg et al. 2012). These features are related to the thermal history of the MS-177 as discussed below.

4.2 Geothermometry

The thermal histories of meteorites have been discussed mainly from silicate and oxide geothermometers. However, most of them cannot be applied to E chondrites because these minerals do not show solid solution in E chondrites. Instead, here we use texture, mineral polymorph, and opaque mineral features to elucidate the thermal history of the MS-177 EL3 fragment (Table 4).

The MS-177 does not show evidence for shock-induced melting such as melt vein and pocket. The texture is different from those of melt rocks as mentioned before. This suggests that the fragment did not experience heating higher than subsolidus temperature, < 1000°C after McCoy et al. (1999). Enstatite is identified as orthoenstatite, indicative of heating under > 600°C after Smyth (1974), assuming that original enstatite in chondrules and their fragments were clinoenstatite as in the case of type 3 E chondrites (Weisberg and Kimura 2012). Although these temperatures depend on pressure, no high-pressure polymorphs in the MS-177 indicate low-pressure conditions, different from the shock vein in A 10164 EH3 chondrite including a high-pressure mineral, coesite (Kimura et al. 2017).

The absence of kumdykolite, high-temperature polymorph of albite, indicates temperatures below ~ 1000°C (Nemeth et al. 2013). The occurrence of quartz without tridymite, cristobalite and others, suggests that temperatures are lower than 900°C (Swamy et al. 1994). In the case of other type 3 E chondrites, silica phases are cristobalite, tridymite, and glass, which crystallized in chondrule melts (Kimura et al., 2005). Therefore, the original silica phases were transformed into quartz in the MS-177 during secondary heating.

Fe-Ni metal and troilite never show eutectic intergrowths, although they commonly occur in close association with each other. This observation indicates temperatures lower than eutectic melting, 970°C (Ryzhenko and Kennedy 1973). Fe-Ni metal often coexists with schreibersite in MS-177, and their compositions indicate temperatures of ~ 800°C, after Zhang and Sears (1996). Perryite was not found in the MS-177. Although its stability is not yet known, it seems that the absence of perryite suggests high-temperature conditions (Kimura et al. 2005).

Troilite commonly contains relatively high Cr contents. This suggests high-temperature conditions of more than 700°C (El Goresy and Kullerud, 1969). Under such conditions, daubreelite is not stable, and it was not found in the MS-177.

The occurrence of keilite, not alabandite, also indicates high-temperature conditions. The composition indicates ~ 600°C for the keilite in MS-177 (Skinner and Luce 1971). Oldhamite contains ~ 2 mol% MgS and MnS components. This also suggests ~ 600°C (Skinner and Luce 1971). The occurrence of buseckite, not rudashevskyite, also supports high-temperature conditions (Ma et al. 2012), although the phase relationships between buseckite and rudashevskyite is not yet clear.

4.3 Thermal history

From the geothermometers mentioned above and from petrographic observations, we discuss the unique thermal history of MS-177. This fragment as well as A-881314 show typical type 3 E chondritic texture. However, the geothermometers mentioned above indicate that MS-177 experienced a high-temperature event under subsolidus conditions, 600–800°C. The wide temperature variation should reflect different closure temperatures of the different geothermometers. Nevertheless, we interpret the geothermometry to indicate that MS-177 experienced a high-temperature event, which took place on the parent body because most minerals show similar high-temperature conditions. This is different from other E3 chondrites where opaque nodules show different thermal histories in each E3 (Lin and El Goresy 2002). After the heating event, MS-177 cooled rapidly because both olivine and silica survive and primary chondrule textures remain. None of the geothermometers indicate low-temperature conditions, supporting this conclusion. The thermal history of the MS-177 is different from equilibrated E chondrites which were heated for long duration (e.g., Kimura et al. 2005).

The lower abundance of schreibersite in MS-177 than in A-881314 is consistent with the high Ni and P contents of the Fe-Ni metal, reflecting a high-temperature event. The low abundance of keilite is explained by the high concentration of Mn in troilite. The absence of daubreelite is consistent with our interpretation of the thermal history. Cr was mostly concentrated into the troilite under high-temperature conditions.

MS-177 contains a lower abundance of olivine than other EL3 chondrites. One possibility is that the olivine reacted with silica to form secondary enstatite under high-temperature conditions. However, we did not observe evidence of secondary enstatite. Although olivine is not abundant in MS-177, the abundance of silica is not different from that of other EL3s. Therefore, the low abundance of olivine is a primary feature, although the possibility of olivine depletion through secondary reactions cannot be totally excluded.

In MS-177, diopside is highly abundant whereas oldhamite is rarely encountered. A possible explanation is that oldhamite reacted with silicate minerals to form diopside during the thermal event on the parent body as mentioned above. Fogel (1997) reported such metamorphic diopside in equilibrated E chondrites. However, diopside in MS-177 does not show the textures expected if it formed from secondary reactions in the parent body. Instead, diopside shows euhedral to subhedral morphologies in chondrules and opaque nodules, suggesting crystallization from the chondrule melts. Ikeda (1989) also reported that diopside crystallized in chondrules in Y-691, EH3 chondrite. A diopside-rich chondrule was reported in the MAC 88136 EL3 (Weisberg et al. 2012). Therefore, we conclude that the abundant diopside in the MS-177 is a primary feature, present in chondrules and opaque nodules before the accretion into the MS-177 parent body.

4.4 Formation process

In summary, the MS-177 EL3 fragment experienced secondary heating under subsolidus conditions on the parent body. The potential heat sources are 1) internal heating by short-lived isotopes, such as ^{26}Al, as suggested for equilibrated O chondrites (e.g., Huss et al. 2006), 2) external heating such as solar-radiation and electromagnetic induction (Huss et al. 2006), and 3) shock-induced heating for short duration which is proposed for heated CM and CR chondrites (e.g., Kimura and Ikeda 1992; Nakato et al. 2008; Mahan et al. 2018). As argued above, metamorphism for long duration by internal heating can be excluded for MS-177. The high temperatures induced by the internal heating is long lasting, 10^6–10^8 years (Miyamoto et al. 1981). In this case, the texture of the MS-177 should have become similar to those of E4-6 chondrites, in which recrystallization degrades chondrule boundaries and olivine disappears. Nevertheless, we cannot totally exclude the possibility that parent body was disrupted into fragments during its high-temperature stage.

It is difficult to assess solar-radiation heating and electromagnetic induction as heat sources. We would need data for implanted solar-wind noble gases. MS-177 would have acquired implanted noble gases by the radiation on the parent body surface in the case of such heating. Additionally, it has been suggested that these heating mechanisms cannot supply enough energy to heat parent bodies (e.g., Huss et al. 2006).

On the other hand, the fragment was heavily shocked as suggested by the shock darkening. A 10164 also experienced a shock event and formed a melt vein. Not only the vein, but the host of A 10164 was heated during the shock event (Kimura et al. 2017). From the observation of A 10164 and the shock features of the MS-177, shock-induced heating seems to the plausible heat source but not to the same degree as A 10164.

Shock-induced heating for a short duration is supported by the survival of olivine and chondrules with sharp outlines. No occurrence of high-pressure minerals indicates that the pressure conditions of the MS-177 were low in comparison with A 10164, which experienced shock-induced partial melting under the conditions of 3–10 GPa and 1000°C (Kimura et al. 2017).

Thus, the thermal history of the MS-177 is unique, differing from the high temperature and pressure conditions for heavily shocked A-10164, and the low-temperature conditions for A-881314 containing Fe-poor alabandite, Mn-Cr-poor troilite, and daubreelite. MS-177 is similar to subgroup b of E chondrites. We suggest that these chondrites and MS-177 experienced similar high-temperature conditions on their parent bodies, although the petrographic features, such as the primary texture, survived during such the high-temperature event because it was a short duration of shock event.

In H3, L3, and LL3 chondrites (UOCs), secondary heating under subsolidus conditions has not been recognized. Unfortunately, appropriate geothermometers especially covering subsolidus conditions, are not common in the case of UOCs. Nevertheless, we expect that some UOCs also experienced secondary heating for short duration like the E chondrites. Opaque minerals may be a key to explore it.

The Almahata Sitta meteorite came from the asteroid 2008 TC3, although the formation of this brecciated asteroid is a controversial problem (e.g., Horstmann and Bischoff 2014). However, urelilitic and chondritic materials were assembled into the parent body, which was a very loosely consolidated (Bischoff et al. 2010). This may suggest that the fragments did not react with each other in the parent body. Therefore, the unique thermal history of the MS-177 originated before final accretion to the Almahata Sitta parent body and developed from the original E chondritic parent body.

5. Summary

We studied the fragment, MS-177, from the Almahata Sitta polymict breccia. This is classified as an EL3 chondrite based on petrographic observations and mineral chemistry. However, it shows unique mineralogical features such as abundant diopside and lack of daubreelite. From the mineral chemistry, MS-177 is also classified as an ELb chondrite, based on the classification scheme proposed by Weyrauch et al. (2018). Many geothermometers suggest that this fragment was subjected to a high-temperature event for a short duration. This may have resulted from a shock event. Enstatite chondrites even type 3, experienced complicated formation processes including shock and thermal events. Some of them were subjected to high-pressure and temperature conditions like A 10164. Others were heated for short duration under subsolidus conditions like MS-177, or not secondarily heated like A-881314. These differences may reflect the shock histories of the E chondrite parent bodies. We need to investigate not only E3 chondrites, but other kinds of type 3 chondrites, to understand whether they experienced secondary thermal and shock histories on the parent bodies. This is significant to explore asteroidal evolution processes.

Declarations

Availability of data and material

Analytical data is available from the corresponding author upon reasonable request.

Competing interests

The authors declare that they have no competing interest.

Funding

This work was supported by a Grant-in-aids of Ministry of Education, Science, Sport, and Culture of Japanese government, No. 18K03729 to M. K.

Authors' contributions

MK carried out the analyses and designed this study. MKW proposed this study. AT, NI, and AY analyzed the data. All authors read and approved the final manuscript.

Acknowledgements

This paper is dedicated to late Prof. A. El Goresy who accomplished the outstanding achievement in meteoritical sciences, especially the research works of E meteorites. The sample of MS-177 was supplied by El Goresy. This work was supported by a Grant-in-aids of Ministry of Education, Science, Sport, and Culture of Japanese government, No. 18K03729 to M. K, National Aeronautics and Space Administration grant #80NSSC18K0589 to MKW. This study was also supported by National Institute of Polar Research (NIPR) through Project research KP307 and General Collaboration Project no. 26-30.

References

Bischoff A, Horstmann M, Pack A, Laubenstein M, Haberer S (2010) Asteroid 2008 TC3—Almahata Sitta: A spectacular breccia containing many different ureilitic and chondritic lithologies. Meteorit Planet Sci 45:1638–1656

El Goresy A, Kullerud G (1969) Phase relations in the system Cr-Fe-S. In: Millman PM (ed) Meteorite Research. D. Reidel, Dordrecht

El Goresy A, Lin Y, Feng L, Boyet M, Hao J, Zhang J, Dubrovinsky L (2012) Almahata Sitta EL-3 Chondrites: Sinoite, Graphite, and Oldhamite (CsS) Assemblages C- and N-Isotopic Compositions and REE Patterns In: Abstracts of the 75th Annual Meeting of the Meteoritical Society, Cairns, Australia, 12–17 August 2012

El Goresy A, Yabuki H, Ehlers K, Woolum D, Pernicka E (1988) Qingzhen and Yamato-691: A tentative alphabet for the EH chondrites. Proc. NIPR Symp. Antarct. Meteorites 1:65–101

Fogel RA (1997) On the siginificance of diopside and oldhamite in enstatite chondrites and aubrites. Meteorit Planet Sci 32:577–591

Horstmann M, Bischoff A (2014) The Almahata Sitta polymict breccia and the late accretion of asteroid 2008 TC3. Chem Erde 74:149–183

Huss GR, Rubin AE, Grossman JN (2006) Thermal metamorphism in chondrites, In: Lauretta, DS, McSween, HYJr (ed), Meteorites and the Early Solar System. The University of Arizona Press

Ikeda Y (1989) Petrochemical study of the Yamato-691 enstatite chondrite (E3) III: Descriptions and mineral compositions of chondrules. Proc. NIPR Symp. Antarct. Meteorites 2:75–108

Imae N, Kimura M, Yamaguchi A, Kojima H (2019) Primordial, thermal, and shock features of ordinary chondrites: Emulating bulk X-ray diffraction using in-plane rotation of polished thin sections. Meteorit Planet Sci 54:919–937

Jones RH (2012) Petrographic constraints on the diversity of chondrule reservoirs in the protoplanetary disk. Meteorit Planet Sci 47:1176–1190

Kimura M, Ikeda Y (1992) Mineralogy and petrology of a unusual Belgica-7904 carbonaceous chondrite: Genetic relationships between the components. Proc. NIPR Symp. Antarc. Meteorites 5:72–117

Kimura M, Lin Y (1999) Petrological and mineralogical study of enstatite chondrites with reference to their thermal histories. Antarct Meteor Res 12:1–18

Kimura M, Weisberg MK, Lin Y, Suzuki A, Ohtani E, Okazaki R (2005) Thermal history of the enstatite chondrites from silica polymorphs. Meteorit Planet Sci 40:855–868

Kimura M, Yamaguchi A, Miyahara M (2017) Shock-induced thermal history of an EH3 chondrite, Asuka 10164. Meteorit Planet Sci 52:24–35

Lin Y, Kimura M (1998) Petrographic and mineralogical study of new EH melt rocks and a new enstatite chondrite grouplet. Meteorit Planet Sci 33:501–511

Lin Y, El Goresy A (2002) A comparative study of opaque phases in Qingzhen (EH3) and MAC 88136 (EL3): Representatives of EH And EL parent bodies. Meteorit Planet Sci 37:577–600

Ma C, Beckett JR, Rossman GR (2012) Buseckite, (Fe,Zn,Mn)S, a new mineral from the Zakłodzie meteorite. Am Miner 97:1226–1233

Mahan B, Moynier F, Beck P, Pringle EA, Siebert J (2018) A history of violence: Insights into post-accretionary heating in carbonaceous chondrites from volatile element abundances, Zn isotopes and water contents. Geochim Cosmochim Acta 220:19–35

McCoy TJ, Dickinson TL, Lofgren GE (1999) Partial melting of the Indarch (EH4) meteorite: A textural, chemical, and phase relations view of melting and melt migration. Meteorit Planet Sci 34:735–746

Miyamoto M, Fujii N, Takeda H (1981) Ordinary chondrite parent body: An internal heating model. Proc. Lunar and Planetary Science Conf. 12B:1145–1152

Nakato A, Nakamura T, Kitajima F, Noguchi T (2008) Evaluation of dehydration mechanism during heating of hydrous asteroids based on mineralogical and chemical analysis of naturally and experimentally heated CM chondrites. Earth Planets Space 60:855–864

Németh P, Lehner SW, Petaev MI, Buseck PR (2013) Kumdykolite, a high-temperature feldspar from an enstatite chondrite. Am Miner 98:1070–1073

Rubin AE, Scott ERD (1997) Abee and related EH chondrite impact-melt breccias. Geochim Cosmochim Acta 61:425–435

Rubin AE, Scott ERD, Keil K (1997) Shock metamorphism of enstatite chondrites. Geochim Cosmochim Acta 61:847–858

Ryzhenko B, Kennedy GC (1973) The effect of pressure on the eutectic in the system Fe-FeS. Am J Sci 273:803–810

Skinner BJ, Luce FD (1971) Solid solutions of the type (Ca,Mg,Mn,Fe)S and their use as geothermometers for the enstatite chondrites. Am Miner 56:1269–1296

Smyth JR (1974) Experimental study on the polymorphism of enstatite. Am Miner 59:345–352

Swamy V, Saxena S, Sundman B, Zhang J (1994) A thermodynamic assessment of silica phase diagram. J Geophys Res 99:11787–11794

Weisberg MK, Ebel DS, Kimura M (2012) Petrology of Chondrules and a Diopside-Rich Inclusion in the MAC 88136 EL3 Chondrite In: Abstracts of the 75th Annual Meeting of the Meteoritical Society, Cairns, Australia, 12–17 August 2012

Weisberg MK, Kimura M (2012) The unequilibrated enstatite chondrites. Chem Erde 72:101–115

Weyrauch M, Horstmann M, Bischoff A (2018) Chemical variations of sulfides and metal in enstatite chondrites-Introduction of a new classification scheme. Meteorit Planet Sci 53:394–415

Zhang Y, Sears DWG (1996) The thermometry of enstatite chondrites: A brief review and update. Meteorit Planet Sci 31:647–655

Tables

Table 1. Modal composition (vol.%) of the MS-177 and average EL3 chondrite.

Mineral	MS-177	EL3 (average)
Enstatite	62.2	65.2
Diopside	3.4	0.3
Olivine	0.4	2.4
Albite	13.6	10.4
Silica	0.7	1.1
Fe-Ni metal	9.4	10.1
Schreibersite	0.2	0.6
Perryite	n.i.	0.1
Troilite	9.7	7.6
Oldhamite	0.3	0.6
Keilite	trace	0.4
Daubreelite	n.i.	0.3
Buseckite	trace	-
Sinoite	0.1	-

n.i.: not identified

Weisberg and Kimura (2012)

Table 2. Representative analyses of silicate phases (wt.%).

Phase	Occurrence	SiO_2	TiO_2	Al_2O_3	Cr_2O_3	FeO	MnO	MgO	CaO	Na_2O	K_2O	Cl	Total	Fo/Wo/An	En/Ab	Fs
Feldspar	Chondrule	62.55	b.d.	22.83	b.d.	0.35	b.d.	0.04	4.88	8.31	0.42	b.d.	99.37	23.9	73.7	2.
Glass	Chondrule	58.45	0.21	23.02	b.d.	0.30	b.d.	0.33	6.66	7.77	0.62	1.73	98.77			
Glass	Chondrule	63.51	b.d.	19.69	0.07	b.d.	b.d.	7.31	4.24	6.15	0.50	0.15	101.64			
Olivine	Chondrule	42.63	b.d.	b.d.	b.d.	0.06	0.15	56.60	b.d.	b.d.	b.d.	b.d.	99.44	99.9		
Diopside	Chondrule	56.05	0.05	0.24	0.07	0.39	0.09	19.03	24.51	0.11	b.d.	b.d.	100.54	51.6	0.6	4
Diopside	Isolated mineral	55.63	b.d.	0.24	b.d.	0.35	b.d.	19.18	24.59	0.15	b.d.	b.d.	100.15	51.8	0.5	4
Enstatite	Chondrule	58.91	b.d.	0.30	b.d.	b.d.	b.d.	39.22	0.49	0.06	b.d.	b.d.	98.98	99.1	0.0	0.
Enstatite	Isolated mineral	60.03	b.d.	0.05	b.d.	0.33	b.d.	39.34	0.47	b.d.	b.d.	b.d.	100.22	98.7	0.5	0.
Quartz	Chondrule	96.62	0.07	0.10	b.d.	0.13	b.d.	0.10	0.08	0.13	b.d.	b.d.	97.22			

b.d.: below detection limits (3s), 0.03 for SiO_2, Al_2O_3, MgO, and CaO, 0.04 for TiO_2, Na_2O, and K_2O, 0.05 for FeO, Cr_2O_3, and Cl, and 0.08 for MnO.

Table 3. Representative analyses of opaque minerals (wt.%).

Phase	Occurrence	Mg	Si	P	S	Ca	Ti	Cr	Mn	Fe	Co	Ni	Cu	Zn	Total
Keilite	Chondrule	2.63	0.05	b.d.	38.25	2.47	0.15	7.11	18.99	24.73	b.d.	b.d.	0.10	0.44	94.92
Fe-Ni metal	Chondrule	b.d.	0.44	0.44	b.d.	b.d.	b.d.	0.06	b.d.	90.13	0.33	7.48	b.d.	0.08	98.94
Fe-Ni metal	Isolated mineral	b.d.	0.42	0.41	b.d.	b.d.	b.d.	b.d.	b.d.	90.31	0.31	7.52	0.11	b.d.	99.08
Oldhamite	Chondrule	0.61	0.20	0.04	40.90	53.28	b.d.	b.d.	1.19	0.77	b.d.	b.d.	b.d.	b.d.	96.99
Schreibersite	Isolated mineral	b.d.	0.06	14.37	b.d.	b.d.	b.d.	0.06	b.d.	77.07	0.24	7.50	b.d.	b.d.	99.30
Buseckite	Chondrule	0.92	0.05	b.d.	33.92	b.d.	b.d.	b.d.	5.00	29.09	b.d.	b.d.	b.d.	26.12	95.09
Troilite	Chondrule	0.08	b.d.	b.d.	36.40	b.d.	0.32	2.41	1.33	57.58	b.d.	0.20	0.07	b.d.	98.40
Troilite	Isolated mineral	b.d.	b.d.	b.d.	36.19	b.d.	0.28	2.14	1.28	58.11	b.d.	0.24	0.09	b.d.	98.34

b.d.: below detection limits (3s), 0.03 for Mg, Si, P, Ti, and Ca, 0.05 for S, Co, Ni, Cr, Mn, Fe, Zn, and Cu.

Table 4. Geothemometries.

Phase	Geothermometry	*Reference*
Metal-Schreibersite	~800 °C	*Zhang & Sears (1996)*
Schreibersite	< 1000 °C	*Doan & Goldstein (1970)*
Perryite	*high-temperature*	*Kimura et al. (2005)*
Keilite	~600 °C	*Skinner & Luce (1971)*
Oldhamite	~600 °C	*Skinner & Luce (1971)*
Buseckite	*high-temperature*	*Ma et al. (2012)*
No daubreelite	≥ 700 °C	*El Goresy & Kullerud (1969)*
No metal-troilite eutectic intergrowth	< 970 °C	*Ryzhenko & Kennedy (1973)*
Quartz	< 900 °C	*Presnell (1995)*
Albite	< 1000 °C	*Nemeth et al. (2013)*
Orthoenstatite	> 600 °C	*Smyth (1974)*
No silicate melting	< 1000 °C	*McCoy et al. (1999)*

Figures

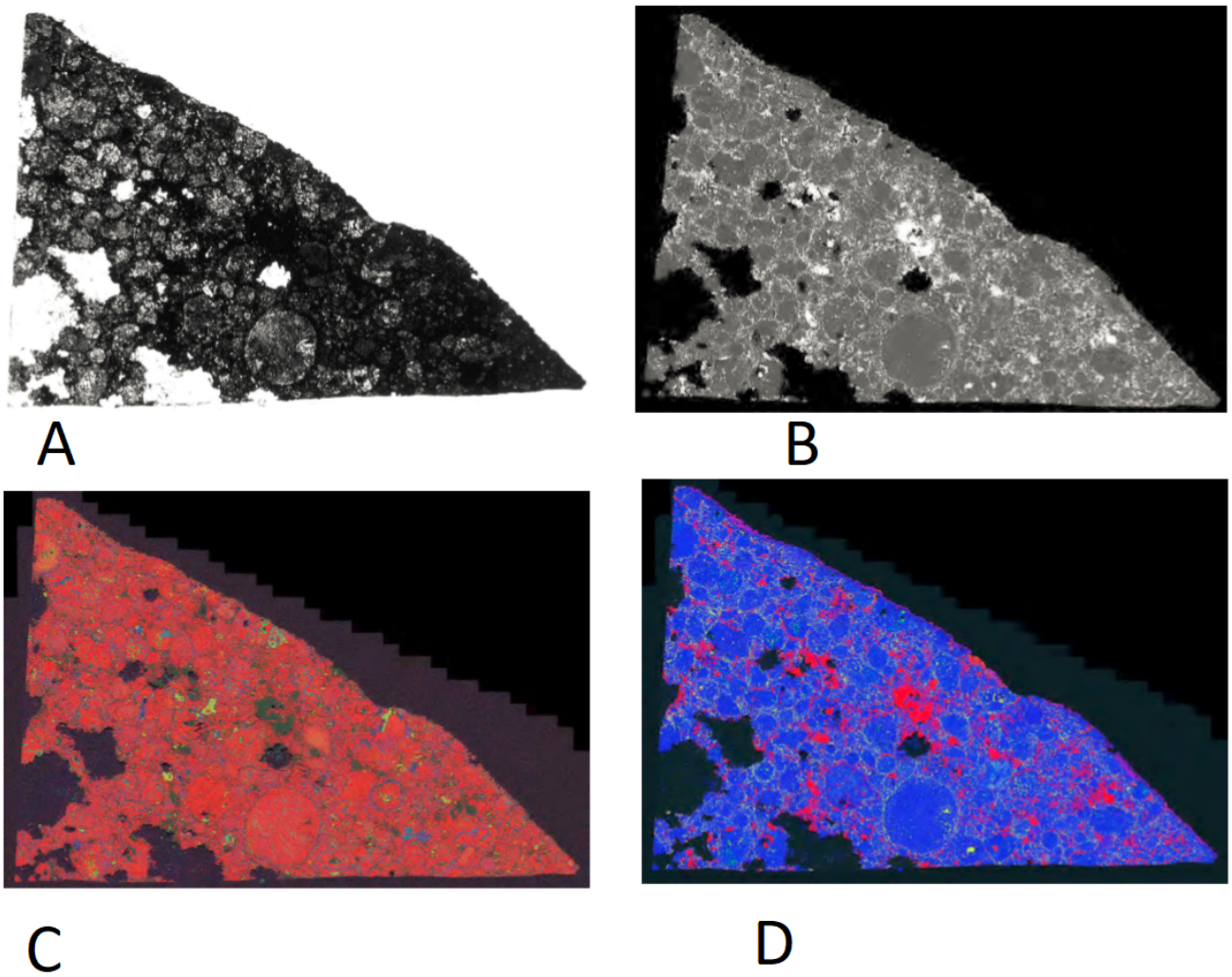

Figure 1

a) Photomicrograph (transmitted light) of a thin section of MS-177. b) Backscattered electron (BSE) image of the section. c) combined elemental map in Mg (red), Ca (green), and Al (blue) showing high abundance of diopside. d) combined elemental map in Fe (red), S (green), and Si (blue) showing high abundance

of Fe-Ni metal nodule. The MS-177 consists of abundant chondrules among isolated silicate minerals, and opaque nodules and isolated minerals. The width of the section is 1.3 cm.

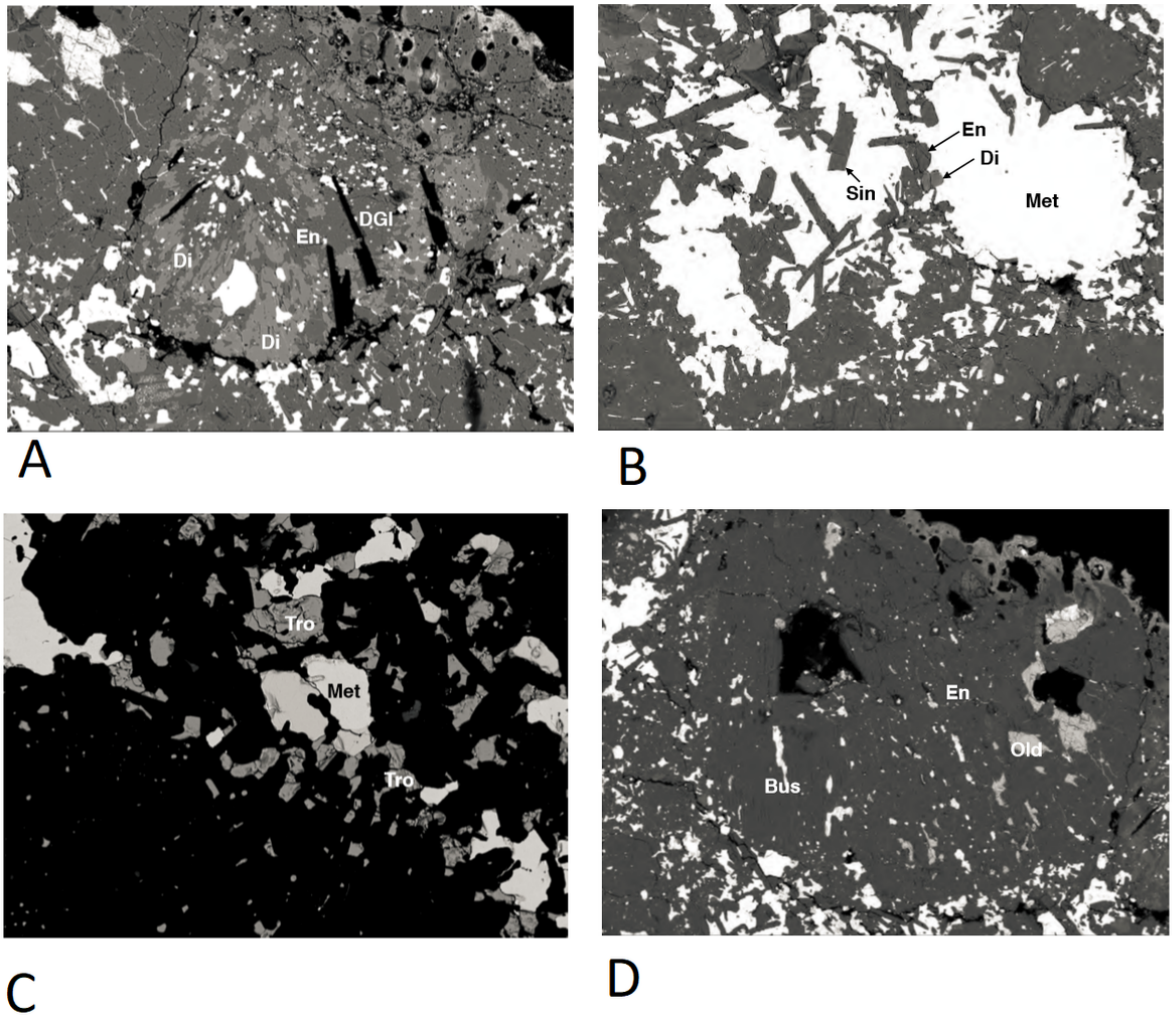

Figure 2

a) BSE image of a chondrule consisting of abundant diopside (Di) with enstatite (En) and devitrified glass (DGl). Width is 490 μm. b) BSE image of an opaque nodule consisting of Fe-Ni metal including laths of enstatite, diopside, and sinoite (Sin). Width is 620 μm. c) BSE image of isolated Fe-Ni metal and troilite. Width is 150 μm. d) BSE image of a chondrule mainly consisting of enstatite with oldhamite (Old) and buseckite (Bus). Width is 820 μm.

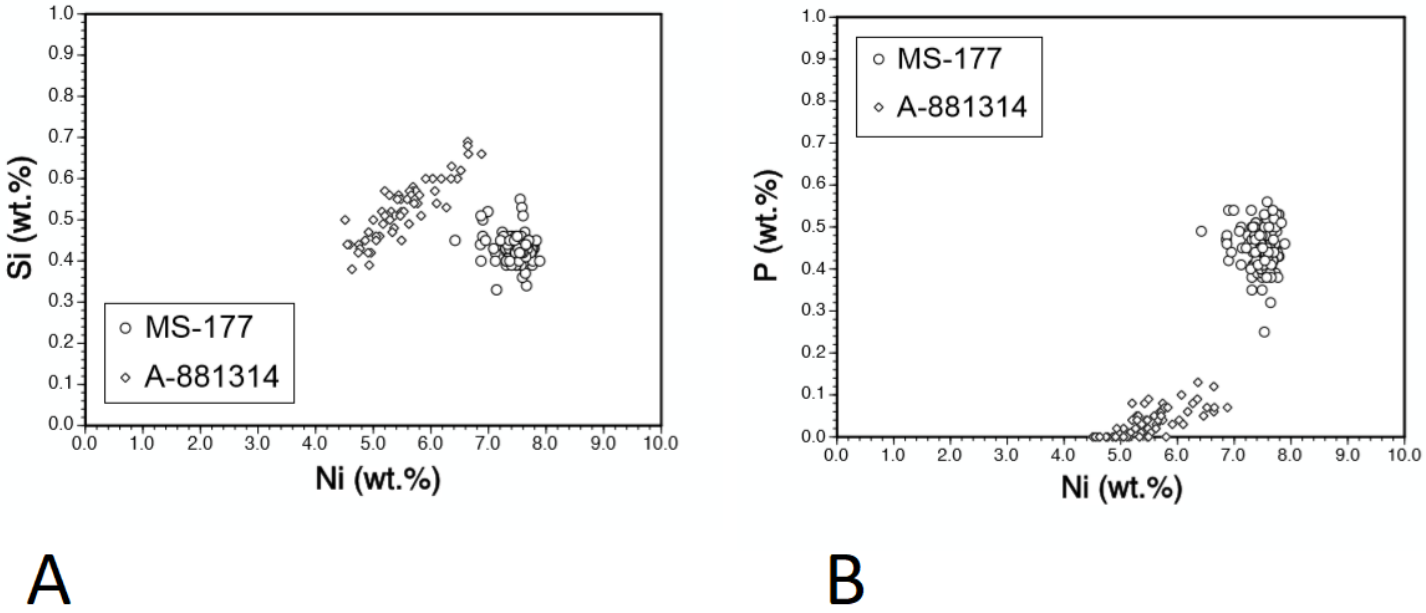

Figure 3

The compositions of Fe-Ni metal on a) Ni versus Si plot, and b) Ni versus P plot.

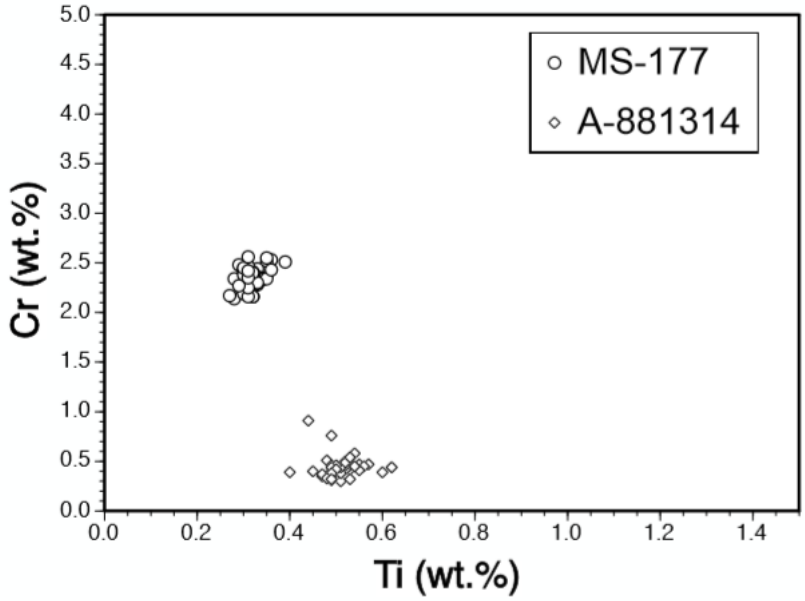

Figure 4

The compositions of schreibersite on Ni versus Si plot.

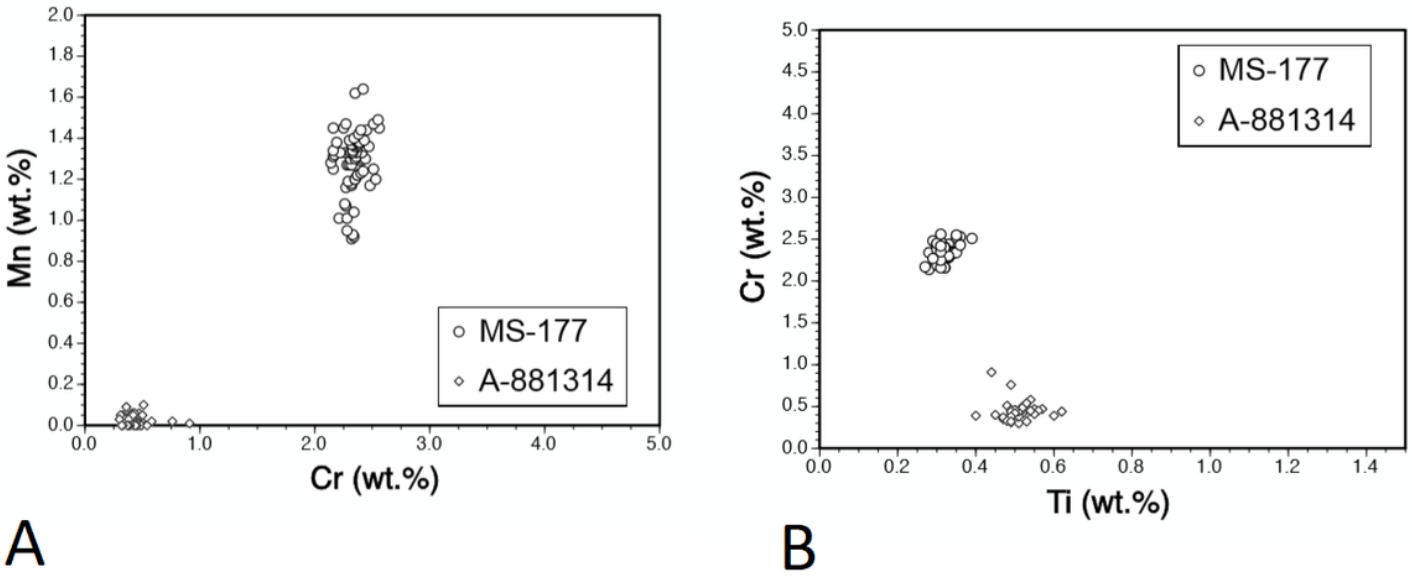

Figure 5

The compositions of troilite on a) Cr versus Mn plot, and b) Ti versus Cr plot.

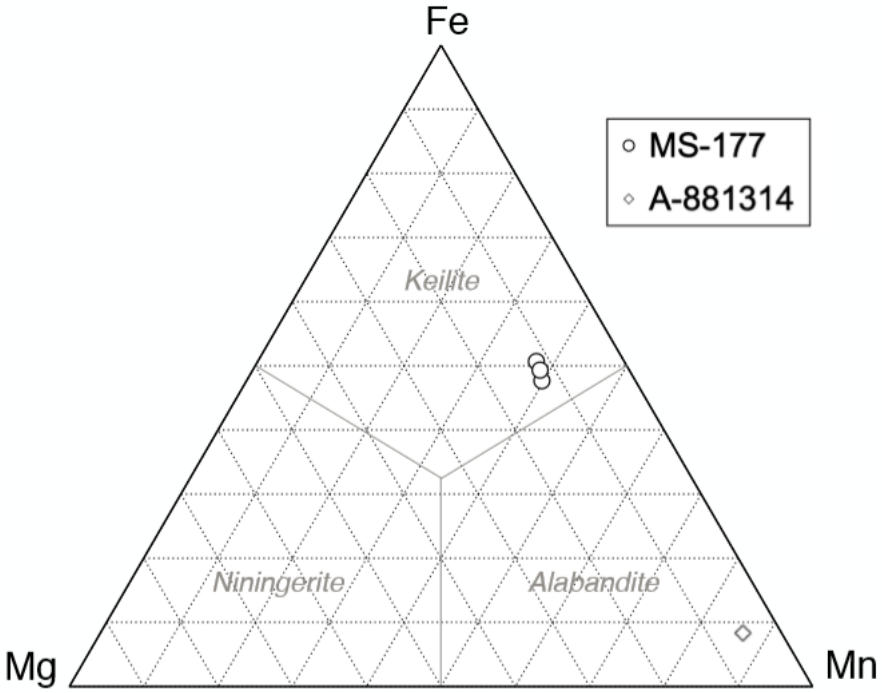

Figure 6

The compositions of (Mg,Mn,Fe) S phases on FeS-MgS-MnS plot (atomic ratio).

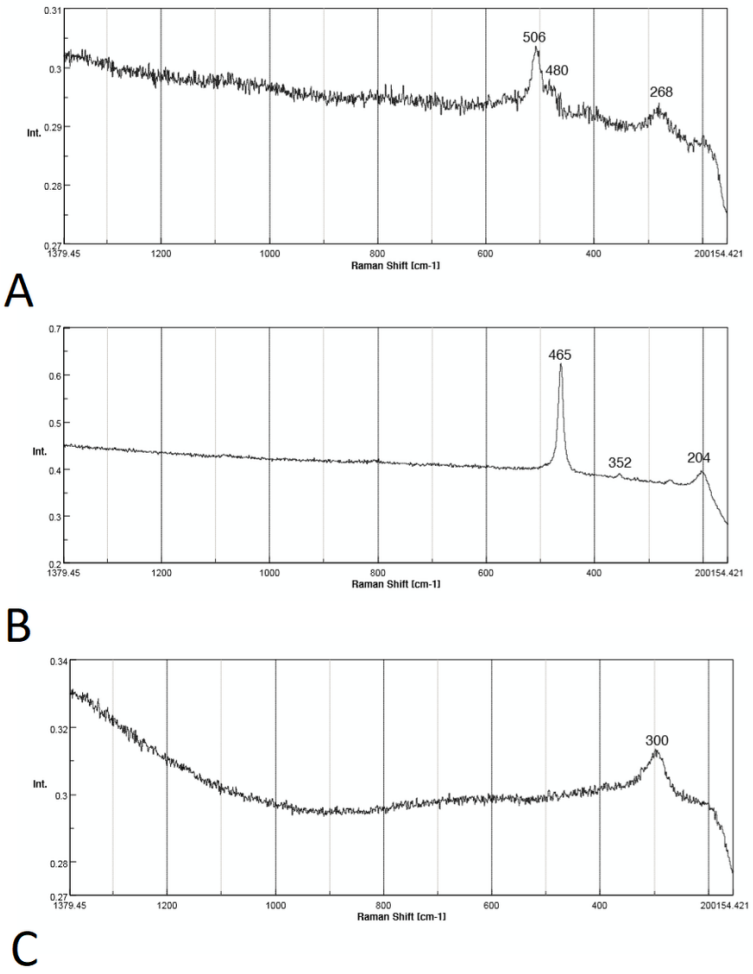

Figure 7

Raman spectra of a) feldspar in a chondrule, b) silica in a chondrule, and c) buseckite in a chondrule.

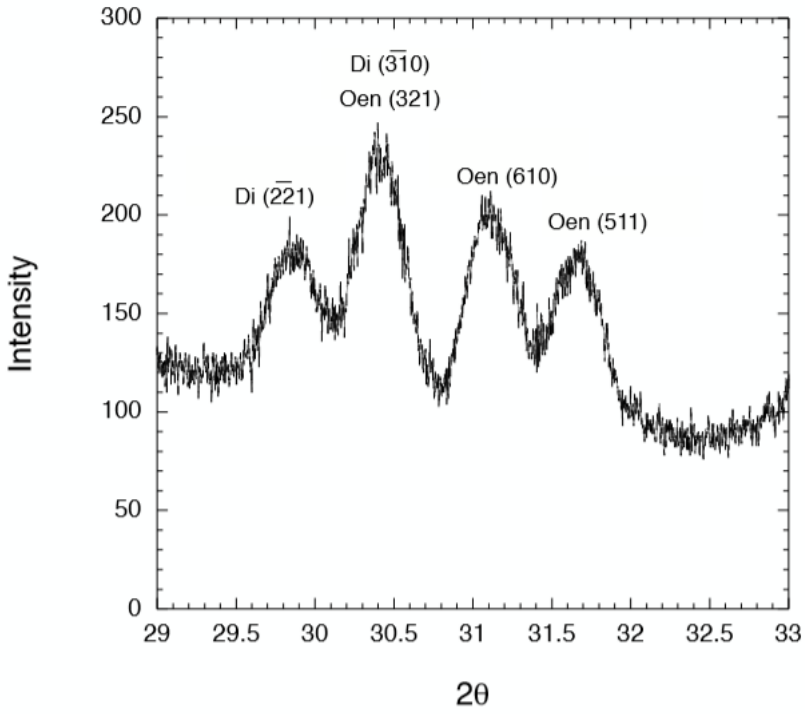

Figure 8

X-ray diffraction of 2 theta, 29-33°. Oen=orthoenstatite and Di=diopside.